Title

NMR Structures of Calmodulin Bound to Two Separate Regulatory Sites in the Retinal Cyclic Nucleotide-Gated Channel

Journal

Biochemistry, 61(18)

ISSN

0006-2960

Authors

Bej, Aritra
Ames, James B

Publication Date

2022-09-20

DOI

10.1021/acs.biochem.2c00378

Peer reviewed

Biochemistry

pubs.acs.org/biochemistry Article

NMR Structures of Calmodulin Bound to Two Separate Regulatory Sites in the Retinal Cyclic Nucleotide-Gated Channel

Aritra Bej and James B. Ames*

Cite This: https://doi.org/10.1021/acs.biochem.2c00378 Read Online

ACCESS | Metrics & More | Article Recommendations

ABSTRACT: Retinal cyclic nucleotide-gated (CNG) channels (composed of three CNGA1 and one CNGB1 subunits) exhibit a Ca^{2+}-induced reduction in channel open probability mediated by calmodulin (CaM). Defects in the Ca^{2+}-dependent regulation of CNG channels may be linked to autosomal recessive retinitis pigmentosa and other inherited forms of blindness. Here, we report the NMR structure and binding analysis of CaM bound to two separate sites within CNGB1 (CaM1: residues 565−589 and CaM2: residues 1120−1147). Our binding studies reveal that CaM1 binds to the Ca^{2+}-bound CaM N-lobe with at least fivefold higher affinity than it binds to the CaM C-lobe. By contrast, the CaM2 site binds to the Ca^{2+}-bound CaM C-lobe with higher affinity than it binds to the N-lobe. CaM1 and CaM2 both exhibited very weak binding to Ca^{2+}-free CaM. We present separate NMR structures of Ca^{2+}-saturated CaM bound to CaM1 and CaM2 that define key intermolecular contacts: CaM1 residue F575 interacts with the CaM N-lobe while CaM2 residues L1129, L1132, and L1136 each make close contact with the CaM C-lobe. The CNGB1 mutation F575E abolishes CaM1 binding to the CaM N-lobe while L1132E and L1136E each abolish CaM2 binding to the CaM C-lobe. Thus, a single CaM can bind to both sites in CNGB1 in which the CaM N-lobe binds to CaM1 and the CaM C-lobe binds to CaM2. We propose a Ca^{2+}-dependent conformational switch in the CNG channel caused by CaM binding, which may serve to attenuate cGMP binding to CNG channels at high cytosolic Ca^{2+} levels in dark-adapted photoreceptors.

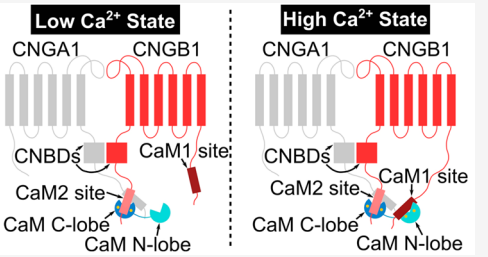

Cyclic nucleotide-gated (CNG) channels in retinal photoreceptors conduct cationic currents modulated by the light-induced depletion of intracellular cGMP that occurs during visual phototransduction.[1−3] Retinal CNG channels are composed of CNGA1 and CNGB1 subunits[4] in which three CNGA1 subunits bind to one CNGB1 in a Ca^{2+}-dependent fashion.[5,6] CNG channels consist of six transmembrane segments (channel domain), a cyclic nucleotide-binding domain (CNBD), and a C-terminal leucine zipper (CLZ) (Figure 1). Upon ligand binding, the CNBD undergoes conformational changes, which open a central hydrophobic gate formed by CNGA1 residues F389 and V393 and CNGB1 residues F872 and I876.[7]

Calmodulin (CaM) binding to retinal CNG channels promotes a Ca^{2+}-induced decrease in channel open probability, which may contribute to light adaptation in retinal rod cells.[8−11] CaM binding decreases the CNG channel-binding affinity for cGMP and causes decreased Ca^{2+} influx.[10,12] Two CaM-binding sites are located in CNGB1 called CaM1 (residues 565−589) and CaM2 (residues 1120−1147) (Figure 1).[6,12,13] CaM1 is required for Ca^{2+}-dependent modulation of the CNGA1/CNGB1 heteromeric channels.[12,14] The function of CaM2 is not known, but CaM2 is located adjacent to the CNBD where it could affect ligand binding.[12] A recent cryoEM structure of the retinal CNG channel revealed that a helix within CNGB1 is bound to the C-terminal domain of CaM (residues 80−149, called the C-lobe).[15] However, the cryoEM structure lacked sufficient resolution to distinguish whether the CaM C-lobe is bound to CaM1 or CaM2, and the CaM N-lobe (residues 1−80) was completely missing in the structure. Defects in the Ca^{2+}-dependent regulation of CNG channels are genetically linked to autosomal recessive retinitis pigmentosa and other inherited forms of blindness.[16] Therefore, elucidating the Ca^{2+}-dependent CNG channel interaction with CaM may provide insights into the treatment of retinal diseases.

In this study, we present NMR structures of CaM bound to CaM1 and CaM2 and provide an analysis of CaM binding to CaM1 and CaM2. Our results suggest that a single CaM could be bound to both sites in CNGB1 in which the calcified CaM N-lobe binds preferentially to CaM1 and the calcified CaM C-lobe binds constitutively to CaM2. Ca^{2+}-free CaM (apoCaM) exhibits very weak binding to CaM1 or CaM2 that is likely not physiologically relevant. We propose that the calcified CaM C-lobe is constitutively anchored to CaM2, which allows CaM

Received: June 25, 2022
Revised: August 22, 2022

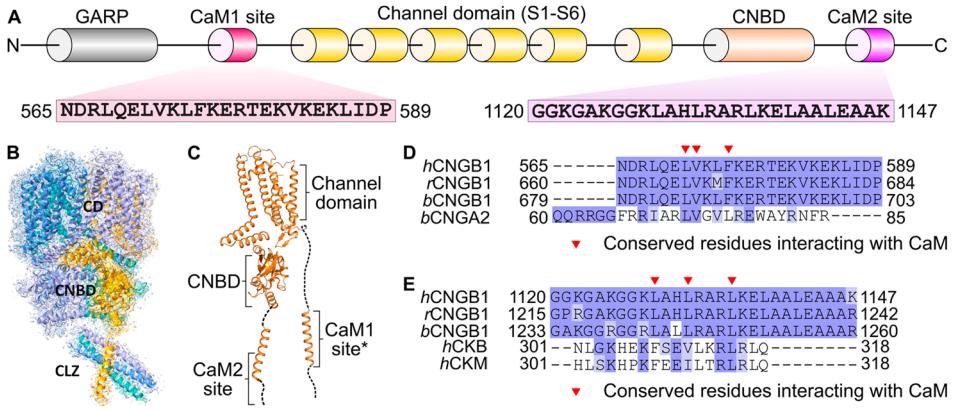

Figure 1. Structural overview of the retinal rod CNG channel. (A) Domain architecture and CaM-binding sites of CNGB1. Amino acid sequences are indicated for CaM1 and CaM2. (B) Cryo-EM structure of the holo CNG channel. CNGA1 subunits are colored blue, cyan, and purple, and CNGB1 is colored orange. Functional domains are labeled as CD (channel domain), CNBD (cyclic nucleotide-binding domain), and CLZ (C-terminal leucine zipper). (C) Ribbon representation of CNGB1. The structure of the CaM1 site was modeled by AlphaFold (asterisk). (D) Sequence alignment of CaM1 (human, rat, and bovine) with the CaM-binding site from CNGA2 (bovine). (E) Sequence alignment of CaM2 (human, rat, and bovine) with the CaM-binding site from creatine kinase (human).

to remain bound to the CNG channel at both high and low Ca^{2+} levels, akin to the CaM preassociation with L-type Ca^{2+} channels.[17,18] The CaM N-lobe is proposed to serve as a Ca^{2+} sensor that binds to CaM1 to promote channel inactivation only at high Ca^{2+} levels in dark-adapted rods.

MATERIALS AND METHODS

Sample Preparation. Recombinant CaM protein samples were prepared and purified as described previously.[19] Peptide fragments of the CaM-binding domains from CNGB1 (CaM1: residues 565−589 and CaM2: 1120−1147) and mutants ($CaM1^{F57SE}$, $CaM2^{L1132E}$, and $CaM2^{L1136E}$) were purchased from GenScript, dissolved in DMSO-d_6, and quantified using UV−vis absorption spectroscopy. A 1.7-fold excess of CaM1 and 3-fold excess of CaM2 peptides were added to Ca^{2+}-bound CaM, incubated at room temperature for 30 min, and concentrated to 0.5 mM.

Isothermal Titration Calorimetry. CaM binding to CaM1 and CaM2 peptides was carried out on a VP-ITC calorimeter (Micro-Cal) at 27 °C as described previously.[20] Samples of Ca^{2+}-bound CaM (injectant) and CaM1/CaM2 peptide (titrant) were prepared by exchanging each into buffer containing 20 mM Tris, pH 7.0, 100 mM KCl, and 1 mM $CaCl_2$. Another sample of apoCaM and CaM2 peptide was prepared by exchanging each into buffer containing 20 mM Tris, pH 8.0, 100 mM KCl, and 2 mM EGTA. The concentration of the CaM1 or CaM2 peptides (including $CaM1^{F57SE}$, $CaM2^{L1132E}$, and $CaM2^{L1136E}$) were each 50 μM in 1.5 mL in the sample cell for titration with 0.5 mM CaM (or CaM lobes) using 34 injections of 7 μL each.

NMR Spectroscopy. Samples for NMR experiments consisted of ^{15}N-labeled or $^{15}N/^{13}C$-doubly labeled Ca^{2+}-bound CaM (0.40 mM bound to CaM1 and 0.50 mM bound to CaM2) bound to unlabeled CaM1 (0.85 mM) or CaM2 peptide (1.2 mM) dissolved in 20 mM Tris-d_{11} (pH 7.0) containing 1 mM $CaCl_2$ and 92%:8% H_2O:D_2O. Samples of unlabeled CaM1 and CaM2 (and mutants) consisted of 40 μM peptide dissolved in 10 mM sodium phosphate at pH 7.0 and 8% D_2O. All NMR experiments were performed at 308 K on a Bruker 600 and 800 MHz Avance III spectrometer equipped with a triple resonance cryogenic TCI probe and pulsed field gradients. Two-dimensional $^{15}N-^{1}H$ HSQC and IPAP-HSQC experiments were performed with 2048 (^{1}H) × 256 (^{15}N) data points. Three-dimensional NMR HSQC-NOESY and HCCH-TOCSY experiments were performed and analyzed as described previously.[21] Spectra were processed using the NMRPipe software package[22] and analyzed using SPARKY.[23]

Residual dipolar couplings (RDCs[24]) of CaM/CaM1 were determined as described previously.[25] Briefly, the filamentous bacteriophage Pf1 (Asla Biotech Ltd., Latvia) was used as an orienting medium. Pf1 (10 mg/mL) was added to ^{15}N-labeled CaM (0.4 mM) bound to unlabeled CaM1 (0.8 mM) to produce weak alignment. $^{1}H-^{15}N$ residual dipolar coupling constants (D_{NH}) were measured using a 2D IPAP (inphase/antiphase) $^{1}H-^{15}N$ HSQC instrument.[26] The backbone N−H RDCs were calculated by measuring the difference in ^{15}N splitting for each amide resonance in both the presence and absence of the orienting medium. The RDC Q-factor and analysis of RDC data were calculated by PALES.[27]

Molecular Docking Calculation. The web-based docking program HADDOCK[28] was used to generate structures of the Ca^{2+}-bound CaM N-lobe and C-lobe each bound to CaM1 and CaM2 peptides, respectively. Crystal structures of the Ca^{2+}-bound CaM N-lobe and C-lobe (from PDB ID: 2F3Y) were docked with helical structures of CaM1 and CaM2, respectively, in order to satisfy the intermolecular distance restraints derived from NMR NOESY data. The template helical structures of CaM1 and CaM2 were each generated using Modeler 9.25 software.[29] The docking calculation was initiated with a rigid body energy minimization that generated 1000 structures. The best 200 structures were subjected to a semiflexible simulated annealing step. In the final step, the 200 structures obtained from the previous simulated annealing step were refined in explicit waters. The coordinate file of the top ranked member in the cluster with the lowest HADDOCK score was chosen for the final structural model displayed in this study. From a total of 200 structures, the 10 lowest energy structures were deposited to the RCSB PDB (PDB ID: 8DGK for CaM/CaM1 and 8DGH for CaM/CaM2). The structure quality was assessed by PROCHECK-NMR[30] and MolProbity.[31]

https://doi.org/10.1021/acs.biochem.2c00378
Biochemistry XXXX, XXX, XXX−XXX

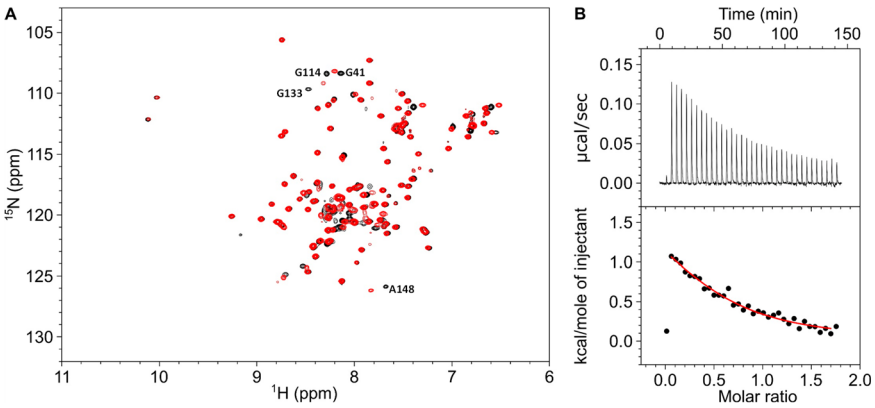

Figure 2. Ca^{2+}-free CaM binding to CaM1 and CaM2. (A) Overlay of $^{15}N-^{1}H$ HSQC spectra of ^{15}N-labeled Ca^{2+}-free CaM in the presence of unlabeled CaM1 peptide (red) versus the absence of CaM1 (black). (B) ITC isotherm of Ca^{2+}-free CaM binding to the CaM2 peptide. Experimental conditions are given in the Materials and Methods section. The ITC data were fit to a one-site model (red line) with $\Delta H = +2.1 \pm 0.4$ kcal/mol and $K_d = 25 \pm 4$ μM.

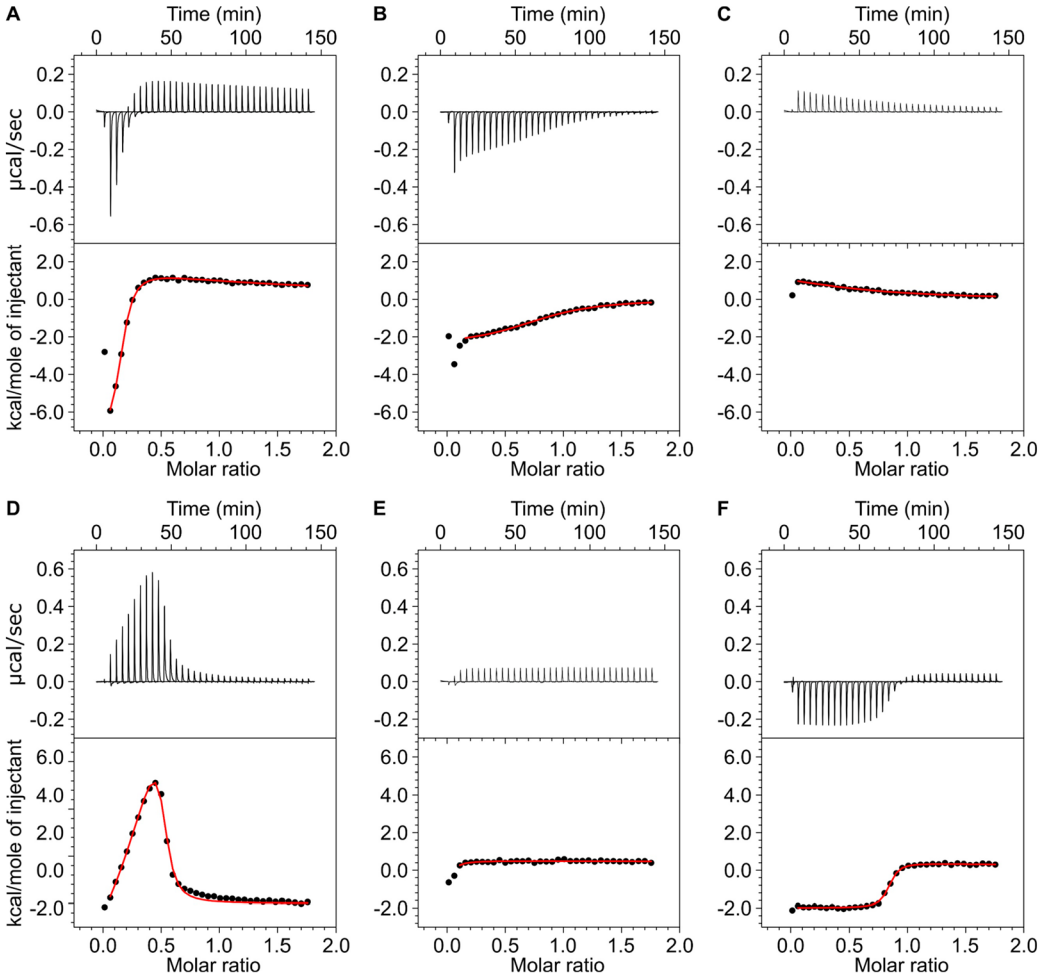

Figure 3. ITC data for CaM binding to CaM1 and CaM2. ITC isotherms of CaM1 binding to (A) full-length CaM, (B) CaM N-lobe, and (C) CaM C-lobe. ITC isotherms of CaM2 binding to (D) full-length CaM, (E) CaM N-lobe, and (F) CaM C-lobe. Each isotherm was fit to either a one-site (in panels B, C, and F) or two-site model (in panels A, D and E), and the binding parameters (ΔH and K_d) are given in Table 1. The CaM1 or CaM2 peptide concentrations were each 50 μM in 1.5 mL in the sample cell for titration with 0.5 mM CaM (or lobes) using 34 injections of 7 μL each.

RESULTS

Ca^{2+}-free CaM Exhibits Very Weak Binding to CaM1 and CaM2. Peptide fragments of CaM1 (residues 565−589) and CaM2 (residues 1120−1147) were shown previously to bind to Ca^{2+}-bound CaM,[6,12] but the binding of CaM1 and CaM2 to Ca^{2+}-free CaM has not been reported. The NMR spectrum of ^{15}N-labeled Ca^{2+}-free CaM in the presence of excess

https://doi.org/10.1021/acs.biochem.2c00378
Biochemistry XXXX, XXX, XXX−XXX

Table 1. ITC Binding Parameters

sample	K_1 (M^{-1})	ΔH_1 (kcal/mol)	K_2 (M^{-1})	ΔH_2 (kcal/mol)
CaM/CaM1	$1.1 \pm 0.1 \times 10^6$	-7.5 ± 0.2	$4.2 \pm 0.5 \times 10^3$	$+40 \pm 4$
CaM C-lobe/CaM1	$3.4 \pm 0.7 \times 10^4$	$+2.0 \pm 0.4$		
CaM N-lobe/CaM1	$1.8 \pm 0.2 \times 10^5$	-2.5 ± 0.2		
CaM/CaM2	$7.3 \pm 1.0 \times 10^6$	-4.5 ± 1.6	$2.9 \pm 0.5 \times 10^6$	$+16 \pm 2$
CaM C-lobe/CaM2	$9.8 \pm 1.0 \times 10^6$	-2.0 ± 0.1		
CaM N-lobe/CaM2	$<1.8 \times 10^4$	$+7.5 \pm 4.0$		
CaM N-lobe/CaM1^{F575E}	$<2.0 \times 10^4$	$+0.7 \pm 0.5$		
CaM C-lobe/CaM2^{L1132E}	$1.8 \pm 0.5 \times 10^4$	$+3.1 \pm 0.5$		
CaM C-lobe/CaM2^{L1136E}	$1.2 \pm 0.7 \times 10^4$	$+2.6 \pm 1.8$		

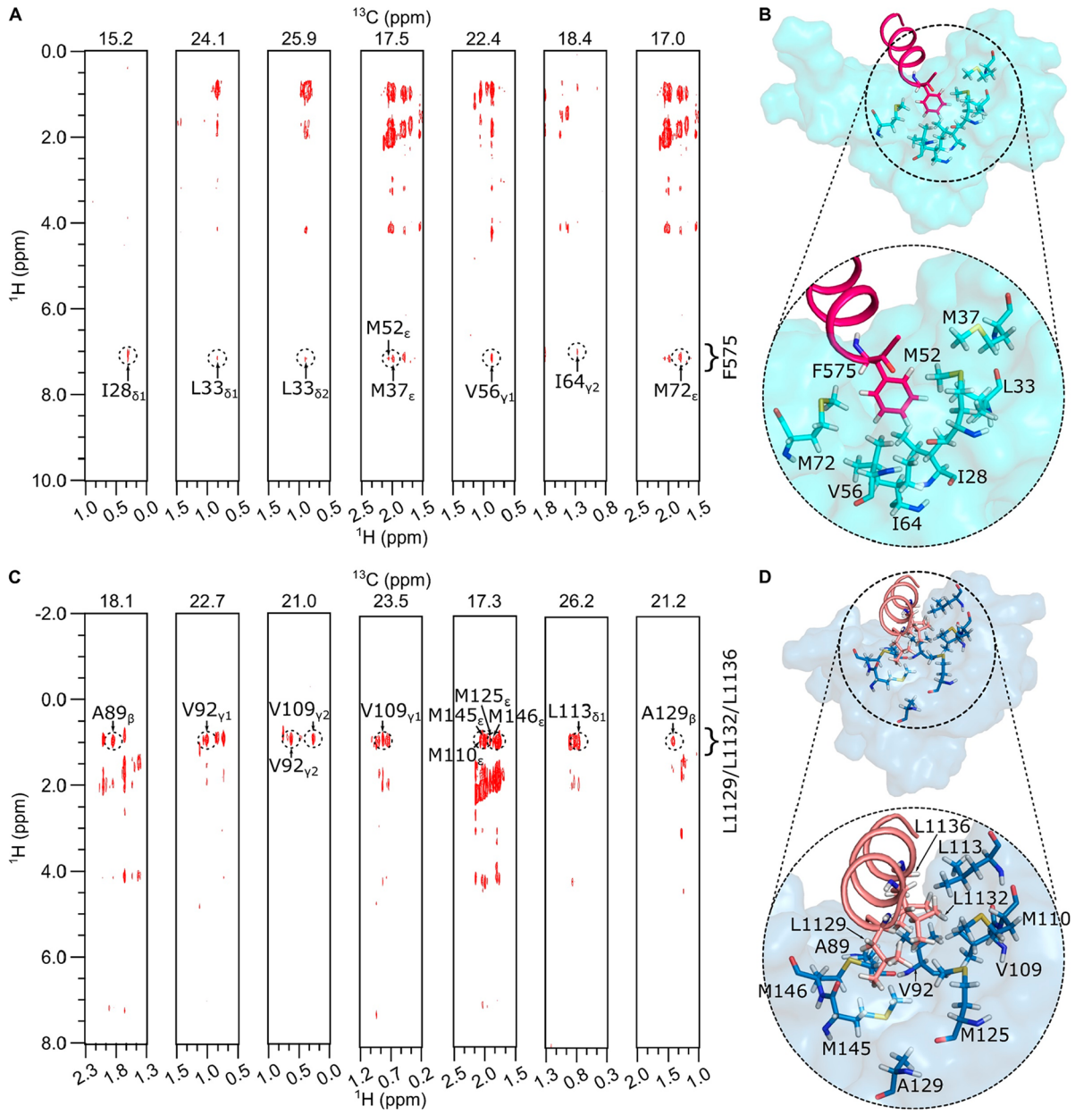

Figure 4. NMR structural analysis of CaM/CaM1 and CaM/CaM2. ^{13}C-edited (F2) and ^{13}C-filtered (F1) NOESY strip plots of ^{13}C-labeled CaM bound to unlabeled peptides of CaM1 (A) or CaM2 (C). The ^{13}C (F2) chemical shift for each plane is shown at the top of each strip plot. The lowest energy space-filling structure of (B) CaM N-lobe (cyan) bound to CaM1 (magenta helix) and (D) CaM C-lobe (dark cyan) bound to CaM2 (light red helix). Side chain atoms of CaM N-lobe residues (I28, L33, M37, M52, V56, I64, and M72), CaM C-lobe residues (A89, V92, V109, M110, L113, M125, A129, M145, and M146), CaM1 residue (F575), and CaM2 residues (L1129, L1132, and L1136) are indicated as sticks in panels B and D.

https://doi.org/10.1021/acs.biochem.2c00378
Biochemistry XXXX, XXX, XXX−XXX

unlabeled CaM1 peptide (Figure 2A, red peaks) looks very similar to the NMR spectrum of Ca^{2+}-free CaM in the absence of CaM1 (Figure 2A, black peaks). More than 95% of the overlaid peaks have identical chemical shifts. However, a few minor spectral changes are likely caused by low fractional binding or by slight differences in sample pH that could affect the amide proton chemical shift of unstructured residues (G41, G114, G133, and A148). The relatively small spectral changes (caused by the addition of CaM1) suggests that Ca^{2+}-free CaM exhibits low fractional binding to the CaM1 peptide and would imply that the dissociation constant (K_d) is greater than the CaM1 concentration (400 μM). By contrast, the addition of CaM1 to Ca^{2+}-bound CaM caused much larger NMR spectral changes,[19] which indicates that CaM1 binds to Ca^{2+}-bound CaM with at least 100-fold higher affinity compared to that of apoCaM (see ITC binding studies below). A similar situation occurs for CaM2. The binding of the CaM2 peptide to CaM was measured by isothermal titration calorimetry (ITC, see Figures 2 and 3). The CaM2 peptide binds to Ca^{2+}-free CaM with K_d equal to 25 $\pm$ 4 μM and ΔH equal to +2.1 $\pm$ 0.4 kcal/mol (Figure 2B). The relatively weak micromolar binding of the CaM2 peptide to Ca^{2+}-free CaM is outside the physiological concentration range of apoCaM (<500 nM[32]) and is in stark contrast to the nanomolar binding of the CaM2 peptide to Ca^{2+}-bound CaM reported below (Figure 3). In summary, both CaM1 and CaM2 exhibited very weak and nonphysiological binding to apoCaM (in contrast to their high-affinity binding to Ca^{2+}-bound CaM), and all studies below were done using Ca^{2+}-bound CaM (referred to below as CaM).

CaM1 Binds to the CaM N-lobe and CaM2 Binds to the CaM C-lobe. Previous studies revealed that CNGB1 has two separate sites (CaM1 and CaM2) that bind to CaM.[6,12,13] Each site could bind to a separate CaM molecule and exhibit a stoichiometry of two CaM bound to one CNGB1. Alternatively, a single CaM might bind to one CNGB1 if the two CaM lobes (from a single CaM) each bind separately to CaM1 and CaM2. Initially, we hypothesized that only one CaM might bind to CNGB1 because the amino acid sequences of CaM1 and CaM2 (Figure 1A) suggest they each adopt an amphipathic helix in which only the hydrophobic side of each helix would bind to a CaM lobe. The amphipathic structure of CaM1 and CaM2 should prevent CaM lobes from binding to both sides of the same target helix, in contrast to the bilobed structures of CaM bound to myosin light chain kinase and other target helices.[33] Therefore, CaM1 and CaM2 are each expected to bind to only one CaM lobe at a time. To test this hypothesis, ITC experiments were performed to monitor CaM binding to CaM1 and CaM2 (Figure 2). The binding of CaM to the CaM1 peptide revealed a biphasic ITC isotherm in which two CaM1 molecules are bound to one CaM molecule at saturation (Figure 3A). The exothermic binding site (ΔH = −7.5 $\pm$ 0.2 kcal/mol) has relatively high affinity with an apparent dissociation constant (K_d) equal to 1.0 $\pm$ 0.2 μM (Table 1). The endothermic binding has much lower affinity with K_d equal to 240 $\pm$ 30 μM. The exothermic binding can be assigned as CaM1 binding to the CaM N-lobe because CaM1 binding to an isolated CaM N-lobe fragment (residues 1−80) is exothermic (ΔH = −2.5 $\pm$ 0.2 kcal/mol) with K_d of 5.7 $\pm$ 1 μM (Figure 3B). The endothermic binding was verified as CaM1 binding to the CaM C-lobe because CaM1 binding to an isolated C-lobe fragment (residues 80−149) is endothermic (ΔH = +2.0 $\pm$ 0.3 kcal/mol) with K_d of 29 $\pm$ 5 μM (Figure 3C). Thus, the ITC results indicate two separate CaM1 molecules bind to CaM to explain the 2:1 binding stoichiometry. Also, CaM1 binds to the CaM N-lobe with at least fivefold higher affinity compared to the CaM1 binding to the C-lobe.

A similar analysis characterized CaM binding to CaM2. The binding of the CaM2 peptide to CaM revealed a biphasic ITC isotherm (Figure 3D) in which two CaM2 molecules are bound to one molecule of CaM at saturation. The higher affinity phase in the isotherm is exothermic (ΔH = −4.5 $\pm$ 1.6 kcal/mol) with K_d equal to 140 $\pm$ 30 nM (Table 1). The lower affinity binding is endothermic (ΔH = +16 $\pm$ 2 kcal/mol). The higher affinity binding can be assigned as CaM2 binding to the CaM C-lobe because the CaM2 peptide binds exothermically to an isolated CaM C-lobe fragment (ΔH = −2.0 $\pm$ 0.2 kcal/mol) with K_d equal to 100 $\pm$ 20 nM (Figure 3F). The lower affinity endothermic binding was verified as CaM2 binding to the CaM N-lobe because the CaM2 peptide binding to an isolated CaM N-lobe fragment is endothermic (ΔH = +7.5 $\pm$ 4 kcal/mol, Figure 3E). It should be noted, however, that a non-stoichiometric and background exothermic heat signal was detected for the CaM N-lobe binding to both CaM1 and CaM2, which is not associated with peptide binding but instead might be an artifact caused by sample heterogeneity of the N-lobe. The ITC results indicate that CaM2 binds to the CaM C-lobe with higher affinity than the CaM N-lobe, in contrast to CaM1 that binds to the CaM N-lobe with higher affinity. These results imply that a single CaM may bind to CNGB1 in which the CaM N-lobe is bound to CaM1 and the CaM C-lobe is bound to CaM2.

NMR-Derived Structures of CaM Bound to the CaM1 Peptide. NMR spectral assignments for the CaM/CaM1 complex were reported previously (BMRB accession number 51222).[19] These previous NMR assignments were used in the current study to obtain NMR-derived intermolecular distance restraints from NOESY data (Figure 4A). The aromatic ring protons assigned to F575 of the CaM1 peptide exhibited strong intermolecular NOESY cross-peaks with side chain methyl resonances assigned to CaM residues (I28, L33, M37, V56, I64, and M72), indicating these atoms of CaM are each less than 5 Å away from the aromatic ring of F575. A total of 21 intermolecular NOESY distance restraints were assigned to residues from the CaM N-lobe, and zero restraints were detected from CaM C-lobe residues. The lack of NOESY cross-peaks assigned to the CaM C-lobe is consistent with its relatively low affinity binding to CaM1 (K_d = 29 μM), which implies a dissociation rate that may be too fast to allow sufficient magnetization transfer during the NOE mixing time. As a result, the NMR data could only define the structure of the CaM N-lobe bound to the CaM1 peptide. Three-dimensional structures of the CaM N-lobe bound to the CaM1 peptide were calculated on the basis of the observed NOESY data (Figure 4A) that served as restraints for molecular docking using HADDOCK[34,35] as described in the Materials and Methods section. The top-ranked docked structure of the CaM N-lobe bound to CaM1 from the cluster with the lowest HADDOCK score is shown in Figure 4B, and structural statistics are provided in Table 2. The overall precision of the 10 lowest energy docked structures is expressed by a root-mean-square deviation (RMSD) of 0.85 $\pm$ 0.16 Å calculated from the coordinates of the main chain atoms (PDB ID: 8DGK). The quality of the docked structures was assessed using PROCHECK-NMR,[30] which shows that >98% of the residues occur in the allowed or favorable regions from the Ramachandran plot and a MolProbity score of 2.3.[31] The structure quality was also verified by the

https://doi.org/10.1021/acs.biochem.2c00378
Biochemistry XXXX, XXX, XXX−XXX

Table 2. Statistics of HADDOCK Docking Calculations

	CaM/CaM1	CaM/CaM2
HADDOCK score	−74.2 ± 1.0	−62.9 ± 3.5
cluster size	195	200
RMSD from lowest-energy structure (Å)	0.7 ± 0.4	0.5 ± 0.3
van der Waals energy (kcal/mol)	−36.5 ± 1.8	−24.8 ± 1.9
electrostatic energy (kcal/mol)	−120.9 ± 7.3	−185.1 ± 14.8
restraints violation energy (kcal/mol)	0.1 ± 0.2	0.4 ± 0.3

residual dipolar coupling (RDC) magnitude and rhombicity that were calculated by fitting the measured residual dipolar couplings to the calculated structure using the PALES program.[27] The docked structures of CaM/CaM1 have a quality Q-factor of 0.27 and an R-factor of 0.95 (Figure 5). The binding

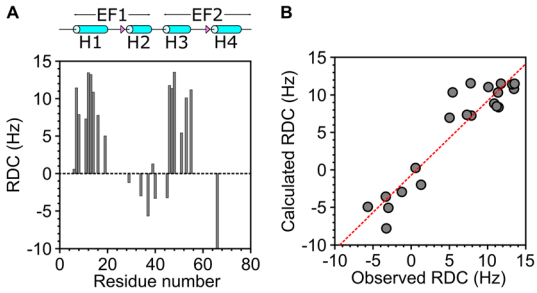

Figure 5. Residual dipolar coupling (RDC) structural analysis of CaM/CaM1. (A) Plot of measured RDC vs residue number. RDCs were measured as the difference in the spectral splitting from $^{1}H-^{15}N$ IPAP-HSQC of ^{15}N-labeled CaM bound to unlabeled CaM1 in the absence of Pf1 (J_{NH}) versus the presence of Pf1 ($J_{NH} + D_{NH}$) as described in the Materials and Methods section. (B) RDCs calculated from the structure of CaM/CaM1 in Figure 4A are plotted versus the RDCs measured from $^{1}H-^{15}N$ IPAP-HSQC spectra. The calculated RDC values show good agreement with the measured values (Q-factor = 0.27 and R-factor = 0.95).

interface between CaM and CaM1 contains many hydrophobic residues of CaM1 (L568, L571, V572, and F575) that make extensive contacts with CaM N-lobe residues (F13, A16, I28, L33, V36, M37, M52, V56, I64, and M72). The structure of the CaM N-lobe (cyan in Figure 4B) bound to CaM1 (magenta helix in Figure 4B) looks similar to the NMR structure of the CaM N-lobe bound to the olfactory CNGA2 peptide,[36] and both structures overlay with an RMSD of 1.1 Å (Figures 6A−C). Conserved residues in CNGA2 (L72, V73, and L76) and CaM1 (L571, V572, and F575) contact the same residues in the CaM N-lobe (A16, F20, L33, V36, M37, L40, M52, I53, V56, I64, and M72) (Figures 6A and B).

NMR-Derived Structures of CaM Bound to the CaM2 Peptide. NMR spectral assignments for the CaM/CaM2 complex were reported previously (BMRB accession number 51447). These NMR assignments were used in the current study to obtain NMR-derived intermolecular distance restraints from NOESY data (Figure 4C). The side chain methyl resonances assigned to L1129, L1132 and L1136 from the CaM2 peptide exhibited strong intermolecular NOESY cross-peaks with side chain methyl resonances assigned to CaM residues (A89, V92, V109, M110, L113, M125, A129, M145, and M146), indicating that these atoms of CaM are each less than 5 Å away from the methyl groups of L1129, L1132 or L1136. A total of 32 intermolecular NOESY restraints were assigned to resonances from the CaM C-lobe. NOESY cross-peaks assigned to residues from the CaM N-lobe had much weaker intensity and were too insensitive to assign. As a result, the NMR data could accurately define only the structure of the CaM C-lobe bound to the CaM2 peptide. Three-dimensional structures of the CaM C-lobe bound to the CaM2 peptide were calculated on the basis of the observed NOESY data (Figure 4C) that served as restraints for molecular docking using HADDOCK[34,35] as described in the Materials and Methods section. The top ranked docked structure of the CaM C-lobe bound to CaM2 from the cluster with lowest HADDOCK score is shown in Figure 4D, and structural statistics are provided in Table 2. The overall precision of the 10 lowest energy docked structures is expressed by a RMSD of 0.56 ± 0.07 Å calculated from the coordinates of the main chain atoms (PDB ID: 8DGH). The quality of the docked structures was assessed using PROCHECK-NMR,[30] which shows that >98% of the residues occur in the allowed or favorable regions from the Ramachandran plot, and a MolProbity score of 2.3.[31] The structure of the CaM C-lobe (dark cyan in Figure 4D) bound to the CaM2 peptide (light red helix in Figure 4D) looks similar to the X-ray structure of the CaM C-lobe bound to a peptide of the creatine kinase CaM-binding domain (CK),[37] and both structures overlay with an RMSD of 0.75 Å (Figures 6D−F) Conserved residues in CK (F308, I311, and L315) and CaM2 (L1129, L1132, and L1136) contact the same residues in the CaM C-lobe (A89, V92, F93, V109, M110, L113, M125, A129, F142, M145, and M146) (Figures 6D and E).

CNGB1 Residues F575, L1132, and L1136 Serve as Linchpin Anchors to CaM. The NMR-derived structure of CaM/CaM1 reveals intermolecular contacts with the CaM1 residue, F575, that points toward the Ca^{2+}-occupied N-lobe of CaM bound to CaM1 (Figure 4B). The side chain atoms of CaM N-lobe residues (F20, I28, L33, M37, M52, V56, and M72) directly contact the aromatic ring of F575 in CaM1. As predicted by this structure, the CaM1 peptide mutant F575E exhibited much weaker binding to the CaM N-lobe compared to $CaM1^{WT}$. The ITC isotherm of $CaM1^{F575E}$ binding to the CaM N-lobe exhibited an endothermic heat signal that did not saturate under the ITC conditions (Figure 7A). A nonstoichiometric exothermic heat signal was also detected for the CaM N-lobe binding to both $CaM1^{WT}$ and $CaM1^{F575E}$, which is not associated with peptide binding but instead is likely an artifact caused by the sample heterogeneity of the N-lobe. The lack of saturation in the ITC isotherm for $CaM1^{F575E}$ indicates that K_d must be at least 10-fold greater than the peptide concentration in the ITC sample cell (K_d > 50 μM). The NMR spectrum of $CaM1^{F575E}$ retains the helical spectral signature seen for $CaM1^{WT}$ (Figure 7D), suggesting that the mutant peptide is structurally intact. Therefore, the F575E mutation weakens the CaM N-lobe binding to CaM1 by over 10-fold and is predicted to disable CaM N-lobe binding to CNGB1 in the full-length CNG channel under physiological conditions.

The NMR-derived structure of CaM/CaM2 reveals intermolecular contacts with CaM2 residues, L1132 and L1136, that are each located on the same side of the CaM2 helix pointing toward the C-lobe of CaM bound to CaM2 (Figure 4D). The side chain atoms of CaM C-lobe residues (A89, V92, F93, V109, M110, L113, M125, A129, F142, M145, and M146) directly contact the side chain methyl groups of L1132 and L1136 in CaM2. As predicted by this structure, the CaM2 peptide mutants L1132E and L1136E each exhibited much weaker binding to the CaM C-lobe compared to $CaM1^{WT}$: K_d was 0.1 ± 0.02 μM for $CaM2^{WT}$, 54 ± 5 μM for $CaM2^{L1132E}$, and 84 ± 10

https://doi.org/10.1021/acs.biochem.2c00378
Biochemistry XXXX, XXX, XXX−XXX

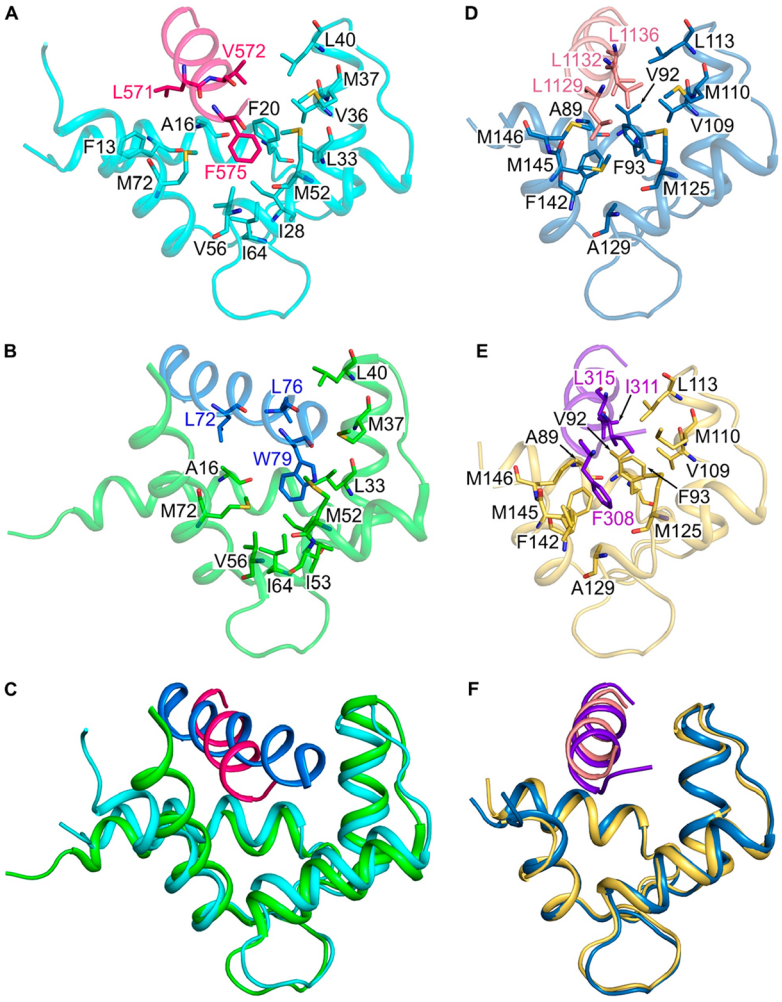

Figure 6. Comparison of CaM/CaM1 vs CaM/CNGA2 and CaM/CaM2 vs CaM/CK. Main chain structures of (A) CaM/CaM1 (PDB ID: 8DGK), (B) CaM/CNGA2 (PDB ID: 1SY9), (D) CaM/CaM2 (PDB ID: 8DGH), and (E) CaM/CK (PDB ID: 7BF2). Main chain structures of CaM/CaM1 overlaid with CaM/CNGA2 (C) and CaM/CaM2 overlaid with CaM/CK (F). The CaM N-lobe (cyan) is bound to CaM1 (magenta helix) in panels A and C; the CaM N-lobe (green) is bound to CNGA2 (blue helix) in panels B and C; the CaM C-lobe (dark cyan) is bound to CaM2 (light red helix) in panels D and F; the CaM C-lobe (yellow) is bound to the peptide fragment of the creatine kinase (CK, purple helix) in panels E and F.

μM for CaM2^{L1136E} (Figures 7B−C). NMR spectra of CaM2^{L1132E} and CaM2^{L1136E} are similar to that of CaM2^{WT} (Figures 7E), suggesting that the mutant peptides are structurally intact. These findings validate our structural model and verify that L1132 and L1136 both make strong contact with the CaM C-lobe. The more than 500-fold decrease in binding affinity caused by the L1132E or L1136E mutations predicts that each of these mutations should disable CaM C-lobe binding to CNGB1 in the full-length CNG channel.

Does Half-Calcified CaM Regulate CNG Channels? The recent cryoEM structure of the retinal CNG channel revealed that a Ca^{2+}-occupied CaM C-lobe was bound to CNGB1 even though the free Ca^{2+} concentration in the cryoEM sample was estimated to be as low as 80 nM.[15] Also, the CaM N-lobe could not be detected in the cryoEM structure, perhaps because the N-lobe was in a Ca^{2+}-free state that binds weakly to CNGB1 and was dynamically disordered (Figure 2). We hypothesize that a half-calcified CaM (two Ca^{2+} bound to the CaM C-lobe, Ca_2/CaMC, and zero Ca^{2+} bound to the CaM N-lobe, CaMN) might be constitutively anchored to CNG channels at the low Ca^{2+} levels (50 nM) found in light-activated photoreceptors.[38] In support of this hypothesis, the nanomolar binding of CaM2 to CaMC is predicted below to cause a more than 10-fold increase in the apparent Ca^{2+} affinity (Scheme 1), which would allow Ca^{2+} to bind to CaMC at the low Ca^{2+} levels found in light-activated photoreceptors. We calculate below that CaMC/CaM2 (Scheme 1) and CaMN/CaM1 (Scheme 2) have apparent K_d values for Ca^{2+}-binding of 60 nM and 0.5 μM, respectively:

Using the Ca^{2+} binding constants for CaMC (K_d = 60 nM) and CaMN (K_d = 0.5 μM), the relative concentrations of Ca^{2+}-free CaM (apoCaM), half-calcified CaM (Ca_2/CaM), and Ca^{2+}-saturated CaM (Ca_4/CaM) each bound to CNGB1 were calculated as a function of free Ca^{2+} concentration (Figure 8). The Ca_2/CaM species (red trace in Figure 8) has 10-fold higher occupancy than Ca_4/CaM at the low Ca^{2+} concentration (50 nM) found in light-activated photoreceptors. Conversely, the Ca_4/CaM species (green trace in Figure 8) has fourfold higher occupancy than Ca_2/CaM at the high Ca^{2+} levels (1 μM) found in dark-adapted photoreceptors. We propose that half-calcified CaM binding to CNGB1 may activate CNG channels in light-activated photoreceptors, whereas fully calcified CaM bound to CNGB1 may inactivate CNG channels at the high Ca^{2+} levels found in dark-adapted photoreceptors (Figure 9).

https://doi.org/10.1021/acs.biochem.2c00378
Biochemistry XXXX, XXX, XXX−XXX

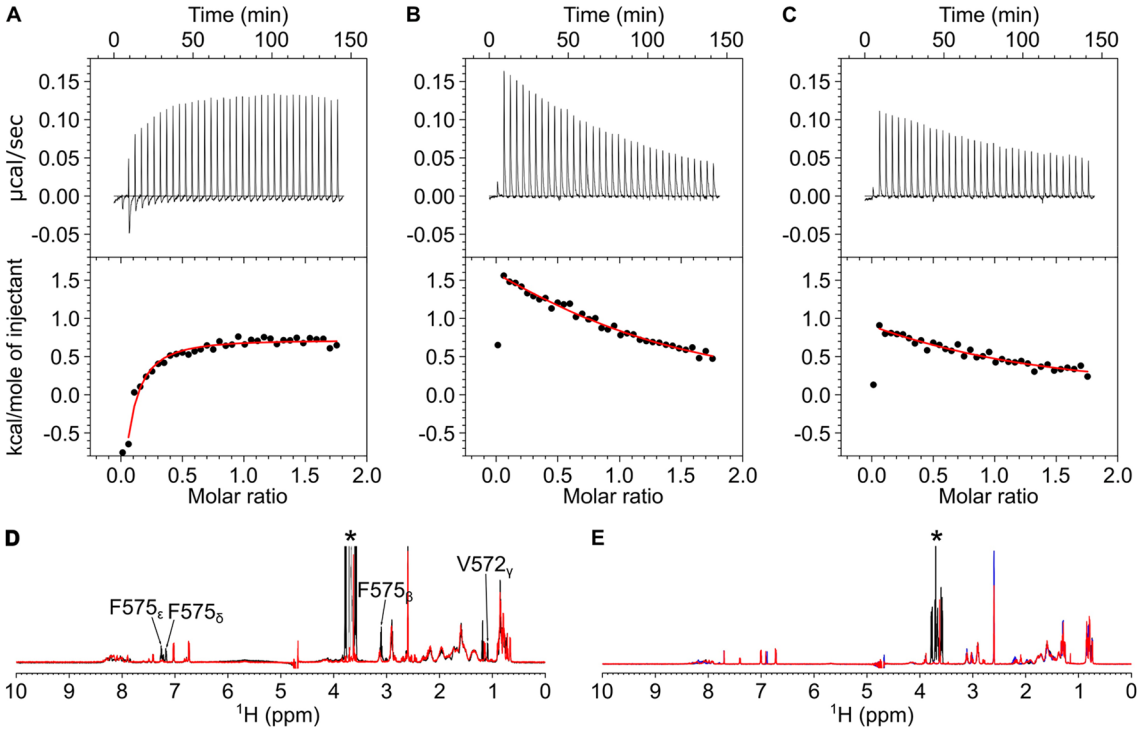

Figure 7. CaM binding to CNGB1 linchpin mutants (CaM1^{F575E}, CaM2^{L1132E}, and CaM2^{L1136E}). ITC isotherms of the CaM N-lobe binding to CaM1^{F575E} (A) and CaM C-lobe binding to CaM2^{L1132E} (B) and CaM2^{L1136E} (C). Each isotherm was fit to a one-site model, and the binding parameters (ΔH and K_d) are given in Table 1. The experimental conditions are provided in the Materials and Methods section. NMR spectra of (D) CaM1^{WT} (black) and CaM1^{F575E} (red) and (E) CaM2^{WT} (black), CaM2^{L1132E} (red), and CaM2^{L1136E} (blue) suggest that CaM1 and CaM2 both form an α-helix and the mutants are structurally intact.

Scheme 1

$$2Ca^{2+} + CaMC \xrightarrow{K_1=10^{12}\ M^{-2}\ 39} Ca_2/CaMC$$

$$Ca_2/CaMC + CaM2 \xrightarrow{K_2=10^{7}\ M^{-1}} Ca_2/CaMC - CaM2 \quad \text{(Fig. 3F)}$$

$$CaMC - CaM2 \xrightarrow{K_3=2.5\times10^{-5}\ M} CaMC + CaM2 \quad \text{(Fig. 2B)}$$

$$CaMC - CaM2 + 2Ca^{2+} \xrightarrow{K_{tot}=K_1\times K_2\times K_3} Ca_2/CaMC - CaM2$$

$$CaMC\ apparent\ K_D = \sqrt{\frac{1}{K_{tot}}} = 60 \pm 20\ nM$$

Scheme 2

$$2Ca^{2+} + CaMN \xrightarrow{K_1=2\times10^{10}\ M^{-2}\ 39} Ca_2/CaMN$$

$$Ca_2/CaMN + CaM1 \xrightarrow{K_2=1.7\times10^{5}\ M^{-1}} Ca_2/CaMN - CaM1 \quad \text{(Fig. 3B)}$$

$$CaMN - CaM1 \xrightarrow{K_3=10^{-3}\ M} CaMN + CaM1 \quad \text{(Fig. 2A)}$$

$$CaMN - CaM1 + 2Ca^{2+} \xrightarrow{K_{tot}=K_1\times K_2\times K_3} Ca_2/CaMN - CaM1$$

$$CaMN\ apparent\ K_D = \sqrt{\frac{1}{K_{tot}}} = 0.5 \pm 0.3\ \mu M$$

DISCUSSION

In this study, our binding data suggest that one CaM is bound to CNGB1 in which the CaM N-lobe binds to CaM1 and the CaM C-lobe binds separately to CaM2 (Figure 3). We also present

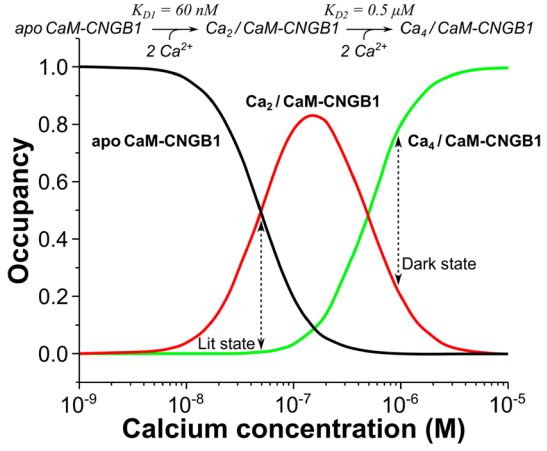

Figure 8. Occupancy of CNGB1-bound CaM species vs [Ca^{2+}]. Concentration profiles of apoCaM bound to CNGB1 (apoCaM-CNGB1, black), half-calcified CaM bound to CNGB1 (Ca_2/CaM-CNGB1, red line), and Ca^{2+}-saturated CaM bound to CNGB1 (Ca_4/CaM-CNGB1, green line). The concentration profiles were calculated according to the kinetic model shown at the top of the plot as described in the Materials and Methods section.

NMR structures of CaM bound to CaM1 (Figure 4B) and CaM2 (Figure 4D). The structure of the CaM N-lobe bound to CaM1 looks similar to the NMR structure of the CaM N-lobe bound to the CaM-binding site within the olfactory CNGA2 (Figure 6C and RMSD = 1.1 Å).[36] However, an important structural difference is that F575 in CaM1 (replaced by L76 in CNGA2) causes the C-terminal end of CaM1 to point downward and alters the orientation of CaM1 relative to

https://doi.org/10.1021/acs.biochem.2c00378
Biochemistry XXXX, XXX, XXX−XXX

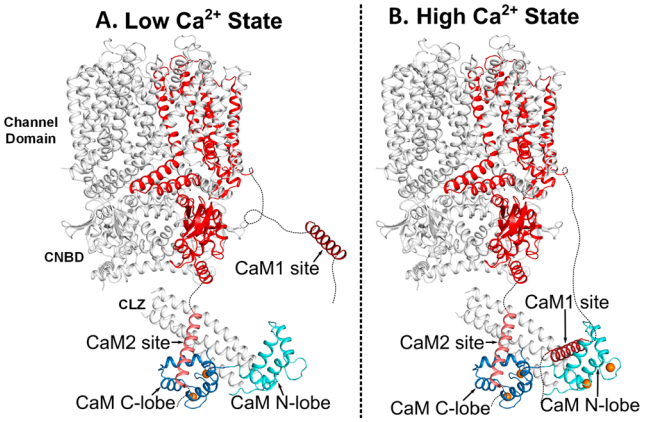

Figure 9. Schematic structural model of CNG channel regulation by CaM. (A) Structural model of the retinal CNG channel[15] in the high-open probability state from light-activated photoreceptors that have low cytosolic Ca^{2+} levels (50 nM). The Ca^{2+}-bound CaM C-lobe (blue) is bound to CaM2 (light red) to promote the high open probability of the channel in the low-Ca^{2+} state. The Ca^{2+}-free CaM N-lobe (cyan) does not bind to CNGB1 and is dynamically disordered in the cryoEM structure.[15] CNGB1 is colored red, and bound Ca^{2+} are orange spheres. (B) Structural model of the retinal CNG channel in the low-open probability state from dark-adapted photoreceptors that have high cytosolic Ca^{2+} levels (1 μM). Ca^{2+}-saturated CaM is bound to both CaM1 and CaM2, which brings CaM1 and CaM2 in close proximity to promote a conformational change in the CNBD that could weaken channel binding to cGMP.

CNGA2. This structural difference may explain why the CaM N-lobe binds to CaM1 with about fivefold lower affinity than it binds to CNGA2.[13] The weaker binding by CaM1 could enable a faster dissociation rate and explain how retinal CNG channels exhibit faster channel regulation (compared to the olfactory CNG channel) to accommodate the fast kinetics of visual phototransduction. The structure of the CaM C-lobe bound to CaM2 looks nearly identical with the crystal structure of the CaM C-lobe bound to CK (Figure 6F and RMSD = 0.75 Å).[37] The only difference is that CaM2 residue L1129 is replaced by F308 in CK. The bulkier aromatic ring of F308 would be expected to make stronger hydrophobic contacts with CaM. However, the CaM C-lobe binds to the CaM2 and CK peptides with nearly the same high affinity (Figure 3F). The nanomolar binding of the CaM C-lobe to CaM2 enhances its Ca^{2+} binding into the nanomolar range (K_d = 60 nM, Scheme 1). This high-affinity Ca^{2+} binding to the CaM C-lobe suggests that a half-calcified CaM species (two Ca^{2+} bound to the CaM C-lobe and zero Ca^{2+} bound to the N-lobe) may bind constitutively to CNGB1 even at low Ca^{2+} levels in light-activated photoreceptors (Figure 8). Mg^{2+} binding to the CaM N-lobe may further stabilize the half-calcified CaM species bound to CNGB1 in light-activated photoreceptors.[40,41] The persistent anchoring of CaM to CNG channels is reminiscent of L-type voltage-gated Ca^{2+} channels that are preassociated with half-calcified and/or Ca^{2+}-free forms of CaM.[17,18,42]

The results from this study suggest a new mechanism for the Ca^{2+}-dependent regulation of retinal rod CNG channels (Figure 9). At high cytosolic Ca^{2+} levels in dark-adapted photoreceptors,[38] we propose that a single Ca^{2+}-saturated CaM binds to CNGB1 (highlighted red in Figure 9) in which the CaM N-lobe binds to the CaM1 site and the CaM C-lobe binds to CaM2 (Figure 9B). In essence, Ca^{2+}-saturated CaM binding to CNGB1 brings CaM1 and CaM2 in close proximity to interact with the C-terminal leucine zipper (CLZ) that in turn might interact with the cyclic nucleotide-binding domain (CNBD) in order to decrease the CNG channel-binding affinity for cGMP.[10,12] At low cytosolic Ca^{2+} levels in light-activated photoreceptors, we propose that Ca^{2+} dissociates from the CaM N-lobe, but Ca^{2+} is suggested to remain bound to the CaM C-lobe (Figures 8 and 9A). This half-calcified form of CaM can still bind to CNGB1 because the CaM C-lobe remains bound to CaM2 even at low Ca^{2+} levels (Figure 9A). The Ca^{2+}-free N-lobe at low Ca^{2+} levels therefore becomes detached from CNGB1 and could explain why the CaM N-lobe is dynamically disordered or otherwise missing in the cryoEM structure.[15] A key prediction of our model is that the CaM C-lobe is constitutively anchored to CNGB1, whereas the CaM N-lobe serves as a Ca^{2+} sensor that undergoes Ca^{2+}-dependent contact with CNGB1. We suggest that Ca^{2+}-induced CaM N-lobe binding to CaM1 may help bridge the CLZ and CNBD to promote a Ca^{2+}-induced reduction in cGMP binding to the CNG channel. Future electrophysiology studies on CNG channels are needed to verify whether CaM binding to both sites (CaM1 and CaM2) is essential for Ca^{2+}-dependent channel function. In particular, the mutations (F575E and L1132E) in the full-length CNG channel should selectively abolish channel binding to the CaM N-lobe and C-lobe, respectively. The F575E mutation should prevent Ca^{2+}-dependent channel inactivation in dark-adapted photoreceptors in contrast to L1132E, which is predicted to destabilize channel opening in light-activated photoreceptors. Lastly, cryo-EM structural studies are needed to determine atomic-resolution structures of retinal CNG channels bound to CaM at both high and low Ca^{2+} levels.

■ ASSOCIATED CONTENT

Accession Codes

Atomic coordinates and structure factor amplitudes have been deposited with the Protein Data Bank as entries 8DGK (CaM/CaM1) and 8DGH (CaM/CaM2).

■ AUTHOR INFORMATION

Corresponding Author

James B. Ames − *Department of Chemistry, University of California, Davis, California 95616, United States;* orcid.org/0000-0003-0934-2595; Email: jbames@ucdavis.edu

Author

Aritra Bej − *Department of Chemistry, University of California, Davis, California 95616, United States;* orcid.org/0000-0002-5561-1891

Complete contact information is available at: https://pubs.acs.org/10.1021/acs.biochem.2c00378

Author Contributions

A.B. performed research, analyzed data, and helped write the paper; J.B.A. directed the project, designed research, and wrote the paper.

Funding

NIH R01 EY012347 (J.B.A.)

Notes

The authors declare no competing financial interest.

https://doi.org/10.1021/acs.biochem.2c00378
Biochemistry XXXX, XXX, XXX−XXX

■ ACKNOWLEDGMENTS

We thank Derrick Kaseman and Ping Yu for help with NMR experiments performed at the UC Davis NMR Facility. This work was supported by NIH grant (R01-EY012347) to J.B.A.

■ ABBREVIATIONS

CaM, calmodulin; CaM1, N-terminal CaM-binding site in CNGB1 (residues 569−589); CaM2, C-terminal CaM-binding site in CNGB1 (residues 1120−1147); CK, CaM-binding site in creatine kinase (residues 301−318); CNGB1, β-subunit from retinal CNG channel; HSQC, heteronuclear single quantum coherence; ITC, isothermal titration calorimetry; NMR, nuclear magnetic resonance; NOESY, NOE spectroscopy

■ REFERENCES

(1) Baylor, D. How photons start vision. *Proc. Natl. Acad. Sci. U.S.A.* **1996**, *93*, 560−565.
(2) Stryer, L. Visual excitation and recovery. *J. Biol. Chem.* **1991**, *266*, 10711−10714.
(3) Fesenko, E. E.; Kolesnikov, S. S.; Lyubarsky, A. L. Induction by cyclic GMP of cationic conductance in plasma membrane of retinal rod outer segment. *Nature* **1985**, *313*, 310−313.
(4) Bradley, J.; Frings, S.; Yau, K.; Reed, R. Nomenclature for ion channel subunits. *Science* **2001**, *294*, 2095−2096.
(5) Shuart, N. G.; Haitin, Y.; Camp, S. S.; Black, K. D.; Zagotta, W. N. Molecular mechanism for 3:1 subunit stoichiometry of rod cyclic nucleotide-gated ion channels. *Nat. Commun.* **2011**, *2*, 457.
(6) Trudeau, M. C.; Zagotta, W. N. Mechanism of calcium/calmodulin inhibition of rod cyclic nucleotide-gated channels. *Proc. Natl. Acad. Sci. U S A* **2002**, *99*, 8424−8429.
(7) Xue, J.; Han, Y.; Zeng, W.; Wang, Y.; Jiang, Y. Structural mechanisms of gating and selectivity of human rod CNGA1 channel. *Neuron* **2021**, *109*, 1302−1313.
(8) Bradley, J.; Reisert, J.; Frings, S. Regulation of cyclic nucleotide-gated channels. *Curr. Opin. Neurobiol.* **2005**, *15*, 343−349.
(9) Fain, G. L.; Matthews, H. R.; Cornwall, M. C.; Koutalos, Y. Adaptation in vertebrate photoreceptors. *Physiol. Rev.* **2001**, *81*, 117−151.
(10) Hsu, Y. T.; Molday, R. S. Modulation of the cGMP-gated channel of rod photoreceptor cells by calmodulin. *Nature* **1993**, *361*, 76−79.
(11) Koutalos, Y.; Yau, K. W. Regulation of sensitivity in vertebrate rod photoreceptors by calcium. *Trends Neurosci* **1996**, *19*, 73−81.
(12) Weitz, D.; Zoche, M.; Korschen, H. G.; Kaupp, U. B.; Koch, K. W. Calmodulin controls the rod photoreceptor CNG channel through an unconventional binding site in the N-terminus of the β-subunit. *EMBO journal* **1998**, *17*, 2273−2284.
(13) Trudeau, M. C.; Zagotta, W. N. Calcium/calmodulin modulation of olfactory and rod cyclic nucleotide-gated ion channels. *J. Biol. Chem.* **2003**, *278*, 18705−18708.
(14) Grunwald, M. E.; Yu, W. P.; Yu, H. H.; Yau, K. W. Identification of a domain on the beta-subunit of the rod cGMP-gated cation channel that mediates inhibition by calcium-calmodulin. *J. Biol. Chem.* **1998**, *273*, 9148−9157.
(15) Barret, D. C. A.; Schertler, G. F. X.; Kaupp, U. B.; Marino, J. Structural basis of the partially open central gate in the human CNGA1/CNGB1 channel explained by additional density for calmodulin in cryo-EM map. *J. Struct Biol.* **2022**, *214*, 107828.
(16) Bareil, C.; Hamel, C. P.; Delague, V.; Arnaud, B.; Demaille, J.; Claustres, M. Segregation of a mutation in CNGB1 encoding the beta-subunit of the rod cGMP-gated channel in a family with autosomal recessive retinitis pigmentosa. *Hum. Genet.* **2001**, *108*, 328−334.
(17) Ames, J. B. L-Type Ca(2+) Channel Regulation by Calmodulin and CaBP1. *Biomolecules* **2021**, *11*, 1811.
(18) Johny, M. B.; Yang, P. S.; Bazzazi, H.; Yue, D. T. Dynamic switching of calmodulin interactions underlies Ca2+ regulation of CaV1.3 channels. *Nat. Commun.* **2013**, *4*, 1717.
(19) Bej, A.; Ames, J. B. Chemical Shift Assignments of Calmodulin Bound to the beta-subunit of a Retinal Cyclic Nucleotide-gated Channel (CNGB1). *Biomolecular NMR assignments* **2022**, *16*, 147−151.
(20) Wingard, J. N.; Chan, J.; Bosanac, I.; Haeseleer, F.; Palczewski, K.; Ikura, M.; Ames, J. B. Structural analysis of Mg2+ and Ca2+ binding to CaBP1, a neuron-specific regulator of calcium channels. *J. Biol. Chem.* **2005**, *280*, 37461−37470.
(21) Lim, S.; Peshenko, I. V.; Olshevskaya, E. V.; Dizhoor, A. M.; Ames, J. B. Structure of Guanylyl Cyclase Activator Protein 1 (GCAP1) Mutant V77E in a Ca2+-free/Mg2+-bound Activator State. *J. Biol. Chem.* **2016**, *291*, 4429−4441.
(22) Delaglio, F.; Grzesiek, S.; Vuister, G. W.; Zhu, G.; Pfeifer, J.; Bax, A. NMRPipe: a multidimensional spectral processing system based on UNIX pipes. *J. Biomol. NMR* **1995**, *6*, 277−293.
(23) Lee, W.; Tonelli, M.; Markley, J. L. NMRFAM-SPARKY: enhanced software for biomolecular NMR spectroscopy. *Bioinformatics* **2015**, *31*, 1325−1327.
(24) Tjandra, N.; Bax, A. Direct measurement of disances and angles in biomolecules by NMR in a dilute liquid crystalline medium. *Science* **1997**, *278*, 1111−1114.
(25) Peshenko, I. V.; Yu, Q.; Lim, S.; Cudia, D.; Dizhoor, A. M.; Ames, J. B. Retinal degeneration 3 (RD3) protein, a retinal guanylyl cyclase regulator, forms a monomeric and elongated four-helix bundle. *J. Biol. Chem.* **2019**, *294*, 2318−2328.
(26) Ottiger, M.; Delaglio, F.; Marquardt, J. L.; Tjandra, N.; Bax, A. Measurement of dipolar couplings for methylene and methyl sites in weakly oriented macromolecules and their use in structure determination. *J. Magn. Reson.* **1998**, *134*, 365−369.
(27) Zweckstetter, M. NMR: prediction of molecular alignment from structure using the PALES software. *Nat. Protoc.* **2008**, *3*, 679−690.
(28) van Zundert, G. C.; Rodrigues, J. P.; Trellet, M.; Schmitz, C.; Kastritis, P. L.; Karaca, E.; Melquiond, A. S.; van Dijk, M.; de Vries, S. J.; Bonvin, A. M. The HADDOCK2.2 Web Server: User-Friendly Integrative Modeling of Biomolecular Complexes. *Journal of molecular biology* **2016**, *428*, 720−725.
(29) Fiser, A.; Do, R. K.; Sali, A. Modeling of loops in protein structures. *Protein science: a publication of the Protein Society* **2000**, *9*, 1753−1773.
(30) Laskowski, R. A.; Rullmann, J. A.; MacArthur, M. W.; Kaptein, R.; Thornton, J. M. AQUA and PROCHECK-NMR: programs for checking the quality of protein structures solved by NMR. *J. Biomol. NMR* **1996**, *8*, 477−486.
(31) Chen, V. B.; Arendall, W. B., 3rd; Headd, J. J.; Keedy, D. A.; Immormino, R. M.; Kapral, G. J.; Murray, L. W.; Richardson, J. S.; Richardson, D. C. MolProbity: all-atom structure validation for macromolecular crystallography. *Acta crystallographica. Section D, Biological crystallography* **2010**, *66*, 12−21.
(32) Wu, X.; Bers, D. M. Free and bound intracellular calmodulin measurements in cardiac myocytes. *Cell Calcium* **2007**, *41*, 353−364.
(33) Hoeflich, K. P.; Ikura, M. Calmodulin in action: diversity in target recognition and activation mechanisms. *Cell* **2002**, *108*, 739−742.
(34) de Vries, S. J.; van Dijk, A. D.; Krzeminski, M.; van Dijk, M.; Thureau, A.; Hsu, V.; Wassenaar, T.; Bonvin, A. M. HADDOCK versus HADDOCK: new features and performance of HADDOCK2.0 on the CAPRI targets. *Proteins* **2007**, *69*, 726−733.
(35) de Vries, S. J.; van Dijk, M.; Bonvin, A. M. The HADDOCK web server for data-driven biomolecular docking. *Nat. Protoc.* **2010**, *5*, 883−897.
(36) Contessa, G. M.; Orsale, M.; Melino, S.; Torre, V.; Paci, M.; Desideri, A.; Cicero, D. O. Structure of calmodulin complexed with an olfactory CNG channel fragment and role of the central linker: residual dipolar couplings to evaluate calmodulin binding modes outside the kinase family. *J. Biomol NMR* **2005**, *31*, 185−199.
(37) Sprenger, J.; Trifan, A.; Patel, N.; Vanderbeck, A.; Bredfelt, J.; Tajkhorshid, E.; Rowlett, R.; Lo Leggio, L.; Akerfeldt, K. S.; Linse, S. Calmodulin complexes with brain and muscle creatine kinase peptides. *Curr. Res. Struct Biol.* **2021**, *3*, 121−132.

https://doi.org/10.1021/acs.biochem.2c00378
Biochemistry XXXX, XXX, XXX−XXX

(38) Nakatani, K.; Koutalos, Y.; Yau, K. W. Ca2+ modulation of the cGMP-gated channel of bullfrog retinal rod photoreceptors. *J. Physiol.* **1995**, *484*, 69−76.
(39) Gilli, R.; Lafitte, D.; Lopez, C.; Kilhoffer, M.; Makarov, A.; Briand, C.; Haiech, J. Thermodynamic analysis of calcium and magnesium binding to calmodulin. *Biochemistry* **1998**, *37*, 5450−5456.
(40) Ohki, S.; Ikura, M.; Zhang, M. Identification of Mg2+-Binding Sites and the Role of Mg2+ on Target Recognition by Calmodulin. *Biochemistry* **1997**, *36*, 4309−4316.
(41) Senguen, F. T.; Grabarek, Z. X-ray structures of magnesium and manganese complexes with the N-terminal domain of calmodulin: insights into the mechanism and specificity of metal ion binding to an EF-hand. *Biochemistry* **2012**, *51*, 6182−6194.
(42) Adams, P. J.; Ben-Johny, M.; Dick, I. E.; Inoue, T.; Yue, D. T. Apocalmodulin itself promotes ion channel opening and Ca(2+) regulation. *Cell* **2014**, *159*, 608−622.

https://doi.org/10.1021/acs.biochem.2c00378
Biochemistry XXXX, XXX, XXX−XXX